A Concertina-Shaped Vibration Energy Harvester-Assisted NFC Sensor With Improved Wireless Communication Range

Kankana Paul, Dinesh R. Gawade, *Member, IEEE*, Roy B. V. B. Simorangkir, *Member, IEEE*, Brendan O'Flynn, *Senior Member, IEEE*, John L. Buckley, *Member, IEEE*, Andreas Amann, and Saibal Roy

***Abstract*—The explosive growth of wireless sensor platforms and their emerging wide range of application areas make the development of a sustainable and robust power source, an essential requirement to enable widespread deployment of these wireless devices. As a solution to this cardinal issue, this article reports the design and fabrication of a resonant vibration energy harvester (VEH) that comprises interleaved springs, manifesting a concertina-shaped structure that can enable large mechanical amplitudes of oscillation. Within a relatively small footprint (9 cm^3), this concertina-VEH yields a large power density of 455.6 $\mu W/cm^3g^2$ while operating at a resonant frequency of 75 Hz. Additionally, the feasibility of the implemented VEH to support near field communication (NFC)-based wireless sensor platform, that is yet uncharted, is also investigated in this work. A very low-power consumption NFC wireless sensor node has been designed and developed for this purpose. The developed concertina VEH has been employed to power the electronics interface of this NFC sensor. Using mechanical energy derived from as low as 0.2-g excitation, our study shows that the VEH can enhance the electromagnetic interaction between the transmitting antenna and the reader, resulting in a 120% increase in wireless communication range for the NFC sensor node. Such a high-performance energy harvester-assisted NFC sensor node has the potential to be used in a wide range of Internet of Things (IoT) platforms as a reliable and sustainable power solution.**

***Index Terms*—Concertina spring, electromagnetic transduction, Internet of Things (IoT), near field communication (NFC) sensor, vibration energy harvester (VEH), wireless communication.**

Manuscript received 7 June 2022; revised 12 July 2022; accepted 25 July 2022. Date of publication 16 August 2022; date of current version 7 December 2022. This work was supported in part by the Platform Research Grant from "CONNECT"—a Strategic Research Centre on "Communication and Future Network-Sustainable IoT" funded by the Science Foundation Ireland (SFI) and co-funded by the European Regional Development Fund under Grant 13/RC/2077_P2; in part by the EU Horizon 2020 Research and Innovation Programme through Project "Enables" under Grant 730957; in part by the European Union's Horizon 2020 Research and Innovation Program through APACHE Project under Grant 814496; and in part by SFI through the European Regional Development Fund under Ireland's European Structural and Investment Funds Programmes 2014–2020 under Grant 12/RC/2289-P2-INSIGHT, Grant 13/RC/2077-CONNECT, Grant 16/RC/3835-VISTAMILK, and Grant 16/RC/3918-CONFIRM. *(Corresponding author: Saibal Roy.)*

Kankana Paul, Dinesh R. Gawade, Roy B. V. B. Simorangkir, Brendan O'Flynn, and John L. Buckley are with the Micro-Nano-Systems Center, Tyndall National Institute, Cork, T12 R5CP, Ireland.

Andreas Amann is with the School of Mathematical Science, University College Cork, Cork, T12 XF62, Ireland.

Saibal Roy is with the Micro-Nano-Systems Center, Tyndall National Institute, Cork T12 R5CP, Ireland, and also with the Department of Physics, University College Cork, Cork, T12 XF62, Ireland (e-mail: saibal.roy@tyndall.ie).

Digital Object Identifier 10.1109/JIOT.2022.3197233

I. Introduction

THE DRIVE toward building pervasive intelligence encompassing urban as well as rural environments has paved the way for the Internet of Things (IoT) [1], which has reshaped our regular lifestyle alleviating the dependence on wired communication systems since its inception [2]. The inexorable advancement in low to ultralow-power electronics have steered the rapid growth of the IoT platform expanding into several application fields, including disaster management [3], agriculture [4], industrial monitoring [5], wearable motion sensing [6], and condition monitoring [7], to name a few. With the ongoing implementation of fifth generation (5G) and the emergence of sixth generation (6G) wireless technology on the horizon, the explosive growth of IoT-connected devices reinforces the requirement of a robust and reliable power solution for the deployed wireless communication platforms. Utilizing distributed clean energy sources, especially the ubiquitous mechanical energy available in the environment through dedicated transducers in the form of vibration energy harvesters (VEHs) to power the IoT-based wireless sensor platforms is a sought-after alternative of batteries in forthcoming IoT applications [8], [9], [10], [11], [12].

Over the past couple of decades, the surge of research in the field of mechanical energy harvesting from ambient vibrations through electromagnetic transducer underpins the simplicity of implementation of this harvester with a spring-mass-damper system [13] along with high mechanical energy extraction efficiency at resonance [14]. For the classical linear type VEHs, the response from the harvester maximizes at resonance when the frequency of excitation equals the natural frequency of oscillation of the energy harvesting unit. The external excitation provided to this harvester translates into relative displacement between the magnet and coil and induces an extractable voltage across the coil terminals. Hence, enhancing the range of mechanical displacement is a potential route to enhance the efficiency of the linear VEH devices at or close to the resonant frequency. Nonlinear spring compliance incorporated into the spring geometry has been exploited in the field of VEHs to widen the operable bandwidth of frequencies [10], enabling the harvester suitable for harnessing mechanical energy from broadband vibrations. Mallick *et al.* [15] reported an FR4-based nonlinear VEH that exploits the nonlinear spring stretching effect (cubic-hardening

stiffness) and demonstrates a five times improvement in the operable bandwidth of frequency. However, the cubic-hardening stiffness-based nonlinear effects strengthen only at higher amplitudes of excitation, which puts a critical limit on the viability of these nonlinear VEHs for relatively weaker vibrations that are predominantly present in bridges, air conditioning systems, trams, trains, etc. [16], [17], [18], [19]. Additionally, depending on the nature of vibration, higher power generation through the nonlinear VEHs is not always guaranteed [20]. However, by virtue of offering wider bandwidth of operable frequencies, instead of peak power delivered for specific frequencies like the linear VEHs, the nonlinear VEHs are promising in providing substantially large average power density over a broadband of frequencies [21] (random vibrations) as compared with the linear VEHs.

On the other hand, the linear type VEHs employing high-efficiency transducers have been used both in academia [22], [23], [24], [25], [26] and in the industry [8], [27] as a robust and reliable solution to the powering issue of wireless sensor platforms. This class of VEH offers large deliverable power at resonance, at the cost of considerably low bandwidth of operable frequencies. However, with an intelligent design strategy, frequency tuning [28], and prior knowledge of the vibration characteristics of the site of deployment [29], the VEH could be designed to trigger the resonance, which effectively results in larger power generation. Qiu *et al.* [30] presented an electromagnetically transduced resonant VEH exploiting the Halbach assembly of magnets which enhances the electromagnetic interaction and maximizes the output power to 90.35 mW with 0.5 g excitation and at a low frequency of resonance (12.65 Hz). Although this device has great potential for powering a wireless sensor platform, however, this comes at the cost of a large footprint (volume of the device, calculated 164.27 cm^3). Gao *et al.* [31] experimentally investigated the performance of resonant VEHs in transducing mechanical energy from wheel-set/track of railways. The device delivers 119 mW power at 6 Hz resonance for a 1.2–2 mm rail track displacement, but occupies a large footprint of 1680 cm^3, which puts a critical limit on its wide range of applicability. Recently Rubes *et al.* [32] presented an autonomous wireless sensing and communication platform powered through an electromagnetic VEH that resonates at 33 Hz with harmonic excitation. The energy harvesting system drives a wireless sensor node to deliver 600 samples of data per second at the cost of a considerably large volume of 124 cm^3. Owing to the geometry of the linear springs, these resonant harvesters perform characteristically small displacements around the point of static equilibrium, which restricts large amplitudes of oscillation for small excitation amplitude. Hence, a key challenge is to develop linear resonators within a small footprint that exhibits large amplitudes of oscillations even for smaller excitations, while demonstrating linear spring-force variation.

From the application perspective, amongst the popular wireless communication platforms such as NarrowBand IoT (NB-IoT), SigFox (a French global network provider), Long-Range Wide Area Network (LoRaWAN), Bluetooth Low Energy (BLE), and Near Field Communication (NFC), the NFC technology offers a unique benefit of a very low power requirement [33] while transmitting data. Recent studies have reported that typically, 900 μW of power is consumed by NFC-based sensor interfaces while offering a communication range up to 4.5 cm [34], [35], [36], [37]. The communication range of the NFC platform largely depends on the several parameters, such as reader type, NFC antenna size, coupling between NFC reader and tag, RFID air interface, and power consumption of the front-end electronics. With NFC type 5 enabled smartphone as a reader, a maximum communication range of 7 cm could be achieved, which increases to 1 m when a 13.56 MHz reader (ISO/IEC 15693) is employed [34], [38]. Nowadays, the inclusion of the NFC technology in smartphones enables on-call data acquisition through reader/smartphones, which substantially reduces the installation cost of the NFC sensors [34], [39]. This allows frictionless migration of the data from the edge to the cloud, which paves the way for a number of low communication-range applications, such as health monitoring [40], food quality monitoring [41], gas monitoring [42], structural health monitoring [43], etc. Battery-assisted NFC sensor node offers enhanced communication range [35]. As the battery powers the front-end electronics associated with the sensor node, the power harvested through the NFC aids in communicating the data-modulated signal by strengthening the electromagnetic interaction between the NFC antenna and the reader. However, the degradation of battery life owing to thermal/mechanical stress as well as chemical reactions [44] poses a great challenge in the usage of batteries for NFC sensor nodes. Hence, assisting the NFC with an energy harvester to power the sensor hardware and to enhance the range of communication appears to be a viable approach that would open wider fields of application.

In this work, we present a novel resonant VEH demonstrator and provide a feasibility study on its potential for supporting wireless sensor platforms to achieve the above-discussed goal. We designed and developed a linear interleaved spring on FR4 material that comprises two linear springs arranged in series, offering a relatively low natural frequency of oscillation ($<$200 Hz) with a small footprint, while exhibiting large out-of-plane oscillations at resonance. Section II outlines the design guidelines and fabrication of the resonant VEH structure that extracts mechanical energy through electromagnetic transduction. Resembling the shape of the musical instrument concertina, the fabricated spring exhibits large displacements while demonstrating linear spring-force characteristics [45], [46]. The electrodynamical characterization of this concertina-VEH is presented in Section III. The resistive load optimization and the frequency response of the VEH for a fixed optimized load have been discussed. Large deformation of the "concertina" spring translates into enhanced voltage induction through the magnet-coil assembly that results in large power delivered across a suitable load for low excitation. As a concept demonstrator, we have designed and developed a low-power NFC sensor node that has been described with functional block diagrams in Section IV. In Section V we demonstrate the efficacy of the developed VEH to power the front-end electronics of the NFC sensor, which

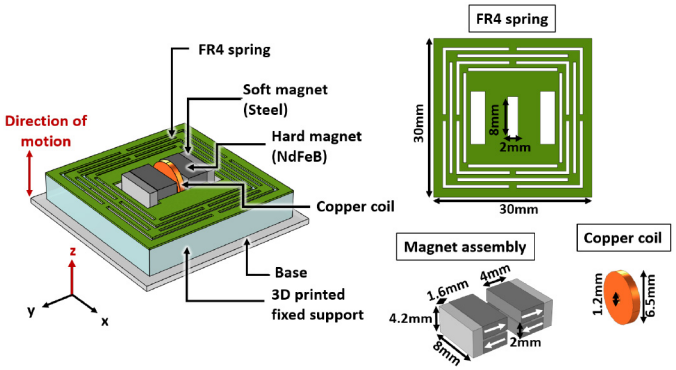

Fig. 1. Schematic of the conceived electromagnetic VEH. The red arrow indicates the out-of-plane motion of the VEH.

strengthens the electromagnetic interaction between the transmitter antenna and the receiver, resulting in an enhanced range of communication. Finally, in Section VI, through an exhaustive comparison we demonstrate the efficacy of the developed VEH in extracting energy from weak vibrations and powering wireless sensor platform offering an improved range of communication. Such a system could be exploited in a wide range of IoT-based applications, e.g., temperature and humidity monitoring of industrial cleanroom environment while extracting mechanical energy from installed air conditioning systems.

II. Design and Fabrication of the Concertina VEH

Typically, an electromagnetic VEH structure comprises a mechanical resonator or a spring that vibrates in response to an externally applied mechanical excitation, and a magnet-coil assembly that is employed to facilitate the electromagnetic transduction. Fig. 1 shows the proposed VEH comprising a spring structure that holds an assembly of magnet on the central stage. The spring is fixed to a rigid support on the base through the outer perimeter and the rest of the spring is suspended and allowed to vibrate. Close to the magnet, a rigidly fixed coil is inserted vertically. On external excitation, the spring vibrates in the vertical direction which enables the magnets to exhibit out-of-plane displacements with respect to the fixed coil, inducing voltage across the coil. In this work, the concertina spring architecture is laser micromachined on a 300 μm thick FR4 sheet. FR4 stands for the low-cost "Flame retardant" materials that are popularly used in printed circuit boards (PCBs) and a wide range of electrical and electronics applications owing to the electrical insulation properties. The low Young's modulus (approximately 21–24 GPa) of the FR4 material aids in scaling the natural frequency of oscillation of the resonator down, enabling the VEH to efficiently harness mechanical energy from ambient vibration sources as a significant fraction of this energy is distributed over the low-frequency domain (<200 Hz) [16], [19]. In addition to the above, the FR4 sheet derives mechanical strength from the constituent interwoven fibreglass, which results in mechanically robust VEH structures. In the literature, FR4-based spring structures have been tested in laboratory vibration environment for more than ten million cycles [53] without any mechanical failure. In another reliability test [54], the FR4 device has been subjected to 100-MPa stress and has been mechanically stable for up to 250 million cycles of operation. Table I shows the comparison of different spring constituent materials. The modulus of elasticity (Young's modulus) parameter, which directly influences the dominant frequency of oscillation of the spring structure, is compared for different materials, including Silicon, Silicon-on-Insulator, Nickel, Copper, Alloy, PDMS, and FR4. Young's modulus of PDMS (360 kPa) and FR4 (21 GPa) structures are significantly lower than the rest of the materials, which, in turn, aids in bringing the frequency of oscillation down to a lower frequency range. However, designing intricate springs on PDMS that would exhibit large out-of-place displacements, could be challenging considering the mechanical stability and durability of the spring architecture. Hence, considering the mechanical robustness, low cost, and low elasticity modulus, we have chosen FR4 as the spring constituent material for the resonant VEH.

TABLE I
Comparison of Spring Materials and Associated Properties of EMVEH Springs

Spring material	Young's modulus	Spring type	Resonant frequency	Max. Disp.
Silicon [47]	*170-190GPa	MEMS	143 Hz 156Hz	0.409 mm 0.351 mm
Silicon-on -insulator [48]	180GPa	MEMS	367 Hz 587Hz	$\sim$ 125 μm (0.5 N) $\sim$ 80 μm (0.5 N)
Nickel[49]	165GPa	MEMS	648 Hz	100 μm (50 mN)
Copper foil [50]	128GPa	Micro-scale	371 Hz	142.4 μm (resonance)
Electroplated copper [51]	*110-130GPa	MEMS	94.5 Hz	259.1 μm (resonance)
PDMS [52]	360kPa	MEMS	93 Hz	$\sim$ 110μm (1.3μN)
FR4 this work	21GPa	Macro scale	75 Hz	2500 μm 2N

*Typical values of Young's modulus of Silicon and Electroplated Copper taken

Four sintered Neodymium-Iron-Boron (NdFeB) magnets are epoxy bonded on the central stage (16 mm $\times$ 10 mm) of the FR4 spring such that oppositely polarized magnets are on each side of the 8 mm $\times$ 2 mm slot at the center dedicated for the coil, as shown in Fig. 1. To intensify the magnetic flux gradient around the coil, soft magnetic steel keepers are used to guide the magnetic flux from the oppositely polarized pair of magnets which aids in forming a closed path of magnetic field lines through the coil. A miniaturized copper wire-wound coil (outer and inner diameter 6.5 and 1.2 mm, respectively, thickness 1 mm, 2500 turns, and 700-Ω resistance) is inserted through the dedicated slot. To keep the coil stationary with respect to the magnets, it is fixed with the base platform through a 3-D printed fixture.

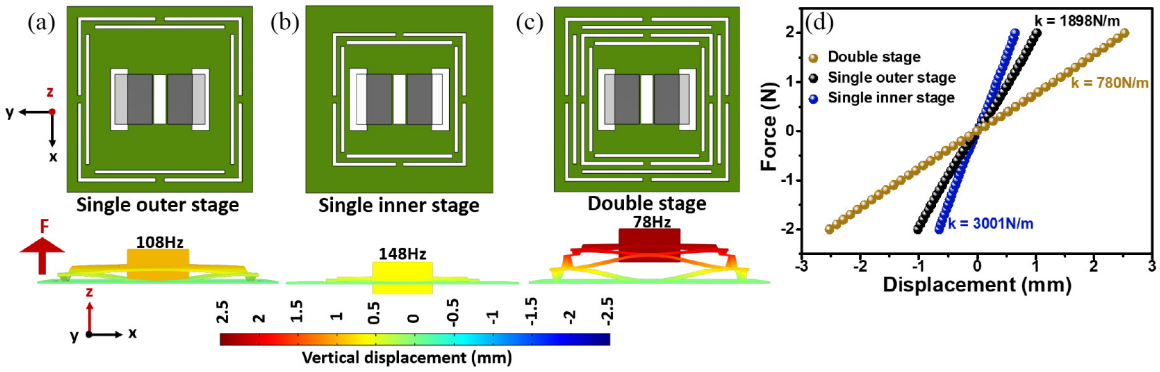

Fig. 2. Design of concertina springs with (a) single stage on the outer side, (b) single stage on the inner side, and (c) double stage springs in series. All have been shown along with the displacement profile for an applied force F. (d) Comparison of the spring force-displacement characteristics for the designed springs.

The spring architecture is designed with the motivation of increasing the out-of-plane compliance to enhance the electromagnetic interaction and hence the extractable electrical energy. The outer dimension of the spring is 30 mm × 30 mm. The width of each spring arm is 0.7 mm. As shown in Fig. 2(a), a single stage of the spring (outer), which comprises four sets of springs, instigates vertical out-of-plane displacement of the central load owing to the interleaved spring architecture. Resembling the shape of the musical instrument "concertina," we call these concertina springs. With a single-stage concertina spring (on the outer side), the VEH exhibits small out-of-plane displacements, as shown in Fig. 2(a), when excited at 108 Hz which is the natural frequency of oscillation of the structure. Approximately 2 N external force is required to displace the load 1 mm normal to the plane. These characteristics manifest a rather stiff spring, yielding a spring stiffness coefficient of 1898 N/m. On the other hand, a single-stage concertina spring on the inner side makes the spring even stiffer and allows the central load to displace only 0.7 mm for a similar level of force at 148 Hz frequency of oscillation, resulting in a large spring stiffness coefficient of 3001 N/m [Fig. 2(b)]. The small displacement exhibited by the single-stage spring restricts the coil from experiencing large magnetic flux variation resulting from the displacement of the magnet assembly.

Adding the interleaved concertina springs in series could potentially enhance the out-of-plane compliance by offering a reduced equivalent spring stiffness (k_{eq}) as compared with the individual single stage of springs [55]. As shown in Fig. 2(c), the second set of concertina springs that are connected in series with the first stage of springs are relatively smaller. The spring stiffness coefficient of the double stage concertina topology reduces to 780 N/m, which is much lower than the stiffness that each of the individual concertina stages offers. The interleaved structure of the spring instigates larger out-of-plane displacements for similar external excitation compared with the rest of the spring topologies, as shown in Fig. 2(d). Arranging these concertina springs in series also helps to scale the frequency of oscillation down from 148 to 78 Hz. In this context, it is to be noted that the patterns and especially the length of the spring (the width of each spring is fixed to 0.7 mm) plays a key role in influencing the spring stiffness and the frequency of oscillation of the structure. This can be verified by revisiting Fig. 2(b), that has the shortest length of springs resulting in larger spring stiffness and higher frequency of oscillation. In contrast with this, the spring with a single stage on the outer end [Fig. 2(a)] demonstrates larger compliance and lower frequency owing to the longer springs, which is further enhanced when two stages of springs are used together in the double-stage concertina design [Fig. 2(c)] that efficiently reduces the spring stiffness as well as the frequency of oscillation. Adding more of such interleaved spring stages could potentially scale down and tune the natural frequency of oscillation of the spring structure as well as further enhance the amplitude of displacement. However, that comes at the cost of the increased footprint of the VEH device. Moreover, very large displacement of the spring from the position of static equilibrium could cast adverse effect on the electromagnetic interaction and hence on the deliverable power, since at very large displacements the magnetic field lines emerging from these small magnets would be too feeble for the coil to interact with. Hence, we limit our study up to the double stage of concertina springs.

Ansys Maxwell has been employed as the finite element analysis tool to investigate the electromagnetic interaction between the coil and the magnet assembly for the different spring topologies using single-stage and double-stage concertina springs, considering open circuit conditions. Following Faraday's law, the relative motion between the coil and the magnet induces a voltage V into the coil which depends on the magnetic flux ϕ and can be represented as follows:

$$V = -N\frac{d\phi}{dt} = -N\frac{d\phi}{dz}\frac{dz}{dt} \tag{1}$$

where N is the number of turns of the coil. Therefore, a larger gradient of magnetic flux would result in higher induced voltage and power. Fig. 3(a) shows the magnetic flux distribution when the VEH is stationary. The arrows indicate the direction of magnetization as well as the magnetic flux lines. The soft magnet blocks on both sides of the magnets aid in routing the magnetic flux lines in a way that intensifies the flux distribution across the coil that is placed at the center. The maximum obtainable out-of-plane displacement has been considered to study the magnetic flux linkage with the coil and the induced voltage into the coil. With a

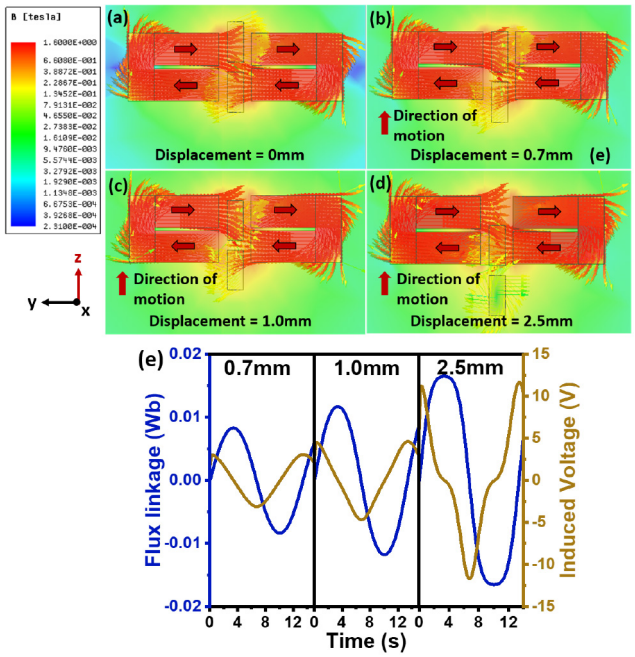

Fig. 3. Electromagnetic interaction between the coil and the magnet assembly and the corresponding variation of magnetic field lines have been shown in (a) for no displacement, (b) for 0.7-mm displacement, (c) for 1-mm displacement, and (d) for 2.5-mm displacements of the magnets from the equilibrium position. (e) Variation of magnetic flux linkage and the induced voltage for different displacement of the magnet.

single stage of concertina spring at the inner side [as shown in Fig. 2(b)] of the spring topology, the maximum displacement is 0.7 mm, which allows 8 mWb magnetic flux linkage, resulting in a maximum of 4-V induced voltage across the coil. This improves when the concertina spring is placed at the outer side of the spring design (maximum displacement 1mm), the magnetic flux linkage enhances to 11 mWb and proportionately the induced voltage increases to 6 V, as shown in Fig. 3(e). The magnetic flux linkage maximizes to 16.5 mWb with double stage concertina springs design that offers large out-of-plane displacement (2.5 mm). Fig. 3(d) shows that with 2.5-mm displacement, the coil segments experience a drastic change of magnetic flux lines through them, yielding a large magnetic flux gradient. This reflects onto the improved induced voltage of 11.2 V. Hence, we have selected the double-stage concertina springs for further analysis and experiments.

The solid mechanics module of COMSOL multiphysics has been used to investigate the modes of vibration of the designed double concertina VEH. We consider here only the first three eigenmodes at 78, 156, and 247 Hz (Fig. 4). The first mode corresponds to the out-of-plane displacement of springs, and the other two modes manifest tilts occurring at higher frequencies. The large difference in frequency of the consecutive modes of vibrations indicates that the concertina springs architecture restricts the torsion or tilts in the system dynamics and promotes the desired out-of-plane vibrations which would aid to enhance the efficiency of the VEH in harnessing mechanical energy.

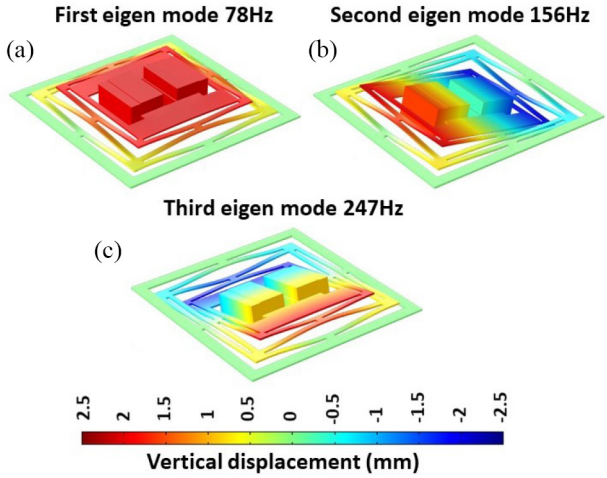

Fig. 4. First three modes of oscillation of the concertina spring structure: (a) at 78, (b) at 156, and (c) 247 Hz. The out-of-plane and torsional modes of vibrations have been portrayed.

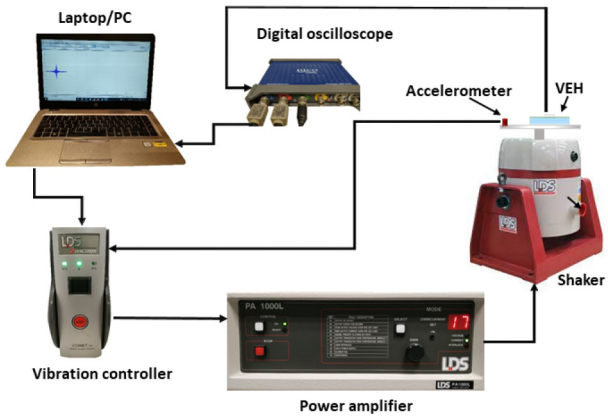

Fig. 5. Schematic of the experimental setup for the electrodynamic characterization of the developed linear concertina-VEH.

III. Experimental Characterization of the VEH and Discussion

The electromechanical characteristics of the conceived VEH have been investigated with Bruel and Kjær Shaker unit that comprises of LDS V455 permanent magnet shaker, LDS vibration controller, PA1000L power amplifier, and a DeltaTron 4517-002 piezoelectric accelerometer mounted on the shaker to monitor the amplitude of excitation and feedback the signal to the controller. The controller in turn generates a signal that is fed to the power amplifier, which then amplifies the signal and sends the drive current signal to the shaker for generating the desired vibrations. The VEH is mounted on the shaker and excited with harmonic vibrations of fixed amplitudes (e.g., 0.1 to 1 g) while the frequency of the excitation is swept from 65 to 85 Hz with a constant sweep rate of 1 Hz/s. The induced voltage across the coil of the VEH is recorded with a digital oscilloscope (Picoscope 3000 series). The experimental setup is shown in Fig. 5.

The frequency of resonance of the VEH is found to be 75 Hz from the initial frequency sweeps in the open circuit conditions, which is slightly lower than 78 Hz resonance as we

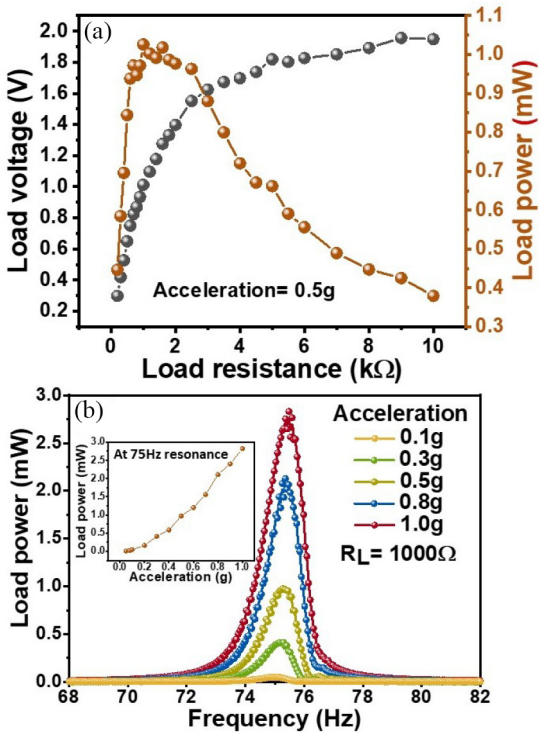

Fig. 6. (a) Variation of load voltage and power delivered across the load with respect to the variation of the resistive load for the developed linear VEH with concertina springs that is shown at the inset. (b) Variation of the power delivered across the optimized resistive load as the frequency of excitation is varied. The inset shows the level of powered delivered to the load as a function of the amplitude of acceleration.

obtained through the finite element analysis. To quantify the sharpness of resonance, or in other words, the linearity of the system, the Q-factor of this VEH has been measured using the ring-down method [56]. The VEH has been excited at the resonant frequency with 0.5 g amplitude of harmonic vibrations. The decay of the response is observed once the excitation is withdrawn. The open-circuit Q-factor is represented as follows:

$$Q_{\mathrm{OC}} = \frac{\pi f_0 \Delta t}{\ln \frac{V_1}{V_2}} = \frac{1}{2\rho_m} \tag{2}$$

where f_0 is the frequency of resonance, V_1 and V_2 are the voltages at the limits of the time interval Δt, and ρ_m is the mechanical damping ratio that is inversely proportional to the Q_{OC}. Using this relation, the Q_{OC} is measured to be 546.17, which in turn indicates a low mechanical damping ratio of 0.0009. These two factors are majorly dependent on the design of the spring and could be further tailored by altering the design.

A suitable resistive load is often connected across the VEH to extract the usable electrical energy for the target applications. In this case, the VEH is driven at the resonant frequency with a fixed amplitude of excitation 0.5 g, and the resistive load across the VEH is varied from 200 Ω to 10 kΩ to find the optimal load condition that will result in maximum power extraction from the VEH. As shown in Fig. 6(a), the power delivered across the resistance maximizes for 1 kΩ load and the delivered power peaks at 1.02 mW for 0.5 g excitation. On increasing the value of the load resistance further, the power gradually drops and the voltage saturates at 1.9 V for a load of 10 kΩ. The variation of the power delivered across the optimal load 1 kΩ with respect to the frequency of excitation, for different amplitudes of the drive has been investigated. For very low amplitudes of excitation, such as 0.1 g, the VEH delivers a low peak load power of 46 μW at 75 Hz [Fig. 6(b)]. On increasing acceleration, the VEH generates more electrical power while resonating at 75 Hz. The VEH delivers a maximum of 2.9 mW power when the amplitude of excitation increases to 1 g, offering a half-power bandwidth of 1.16 Hz. The inset of Fig. 6(b) shows the variation of the obtainable power at 75 Hz as a function of the amplitude of excitation. It is noticeable that the power increases steeply with the acceleration, with approximately a rate of 300 μW of additional power for increasing the acceleration by 0.1 g. The high out-of-plane compliance of the double-stage concertina spring structure aids in enhancing the electromagnetic interaction, which translates into large extractable power from a considerably small footprint.

TABLE II
COMPARISON OF WIRELESS COMMUNICATION TECHNOLOGIES

Wireless Technology	Wireless comm. range(m)	DC Sleep current (μW)	Tx RF power (mW)	Reference (mW)
NB-IoT	10000	10	252-900	[58], [59]
SigFox	10000	2.1	66	[58], [60]
LoRaWAN	5000	2.2	103-264	[58], [61]
WiFi	250	13.2	775.7	[58], [62]
ZigBee	100	2.97	115-152	[58], [63]
BLE	20	2.91	21.12	[64], [65]
NFC	0.07	2.34	0.198	[38]

IV. DESIGN AND FABRICATION OF THE NFC-BASED SENSOR NODE

The objectives of the target application primarily influence the selection of wireless technology. NB-IoT, SigFox, LoRaWAN, WiFi, and ZigBee are among popular commercial wireless communication solutions that offer a long range of communication at the cost of higher transmission power requirement. However, the widespread usage of smartphones that typically comprise embedded BLE and NFC plays a key role behind the popularity of these two wireless technologies, which allows on-call data acquisition wirelessly within a shorter communication range. In particular, the NFC technology, that has been used for this work, is a short range and contactless communication technology that outperforms BLE in terms of power requirement. We summarize and compare the key performance metrics of the different wireless technologies in Table II.

The NFC technology exploits inductive coupling between two loop antennas in close proximity to facilitate reliable data communication, and operates within the worldwide available unlicensed radio frequency band of 13.56 MHz [57]. A block diagram of a battery-less NFC temperature and relative humidity sensor with a reader (in this case NFC type 5 enabled smartphone) is shown in Fig. 7. The role of the smartphone in this setup is to wirelessly power the sensor and

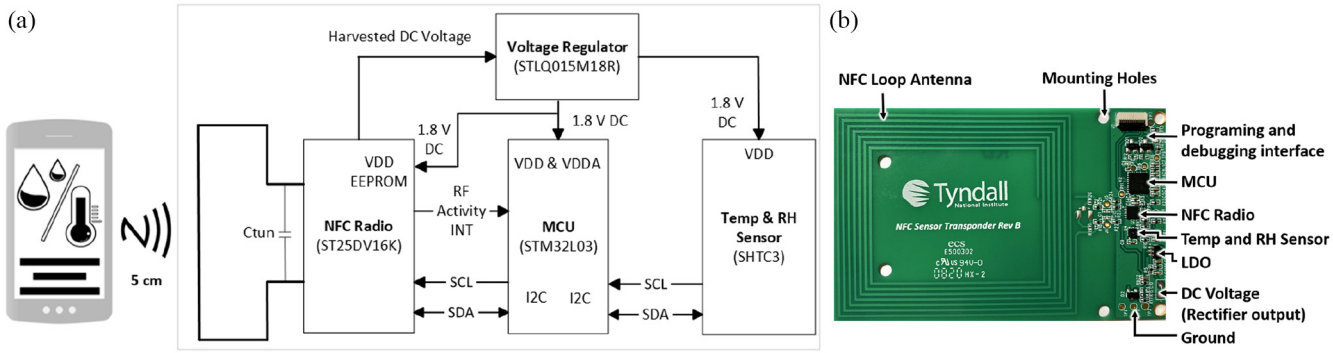

Fig. 7. (a) Functional block diagram of the NFC sensor hardware. (b) Developed NFC sensor hardware [34].

also to wirelessly read the data that the sensor generates. In principle, upon placing the smartphone near the NFC sensor hardware, the time-varying electromagnetic fields generated from the NFC transmitter of the smartphone [shown in Fig. 7(a) through the signal symbol] induces current into the NFC loop antenna in the sensor hardware through inductive coupling. A fraction of the harvested RF power is employed to power the front-end electronics of the sensor and the remaining power is used to facilitate the communication of the data acquired by the sensor through the NFC radio. The detailed process is illustrated in Fig. 7(a). As shown, the loop antenna feeds the induced RF power to the NFC radio transceiver. The RF front-end of this NFC radio consists of energy harvesting circuitry, which converts the harvested RF power into the DC voltage. Following this RF-DC conversion, a low dropout voltage regulator (LDO) is used to regulate this incoming DC voltage into a steady DC supply (i.e., 1.8 VDC) for the following sensor electronics stage, e.g., the microcontroller unit (MCU), the sensor, and all other circuitry. Once the required power is received, the sensor is activated and can function to measure the target physical parameters, such as temperature, relative humidity, and so on. Through I2C protocol the sensor communicates this acquired data with the MCU using the remaining RF power that was harvested through the smartphone. This data is then written into the user area of NFC radio's dual access nonvolatile memory (EEPROM) and it is read through the smartphone wirelessly using the dedicated read command. The time taken by the NFC sensor node from harvesting the power from the reader to communicating the data back to the reader is often referred as tapping time, which is dependent on the computational speed of the microcontroller and the data transmission rate. The voltage and clock settings have been optimized [i.e., Clock source = Multispeed internal oscillator clock, MCU peripheral clock (f_{CLK}) = 0.524 MHz, I2C core input clock (f_{2CIN}) = 1.028 MHz, core voltage (V_{CORE}) = 1.2 V, and supply voltage (V_{DD}) = 1.8 V] considering the tradeoff between the computational speed and DC power consumption. The DC power required by the NFC sensor hardware to be fully functional is measured to be 597 μW which is considerably reduced with respect to the previously reported value of 900 μW [34]. Our developed NFC sensor [Fig. 7(b)] requires a minimum tapping time of 6.79 s.

The NFC sensor hardware prototype is shown in Fig. 7(b), which comprises a loop antenna and the following commercial off-the-shelf (COTS) components: an NFC radio (ST25DV16K-JFR6D3), MCU (STM32L031K6U6), and LDO (STLQ015M18R) from STMicroelectronics, as well as temperature and humidity sensors (SHTC3) from Sensirion AG. The sensor hardware uses a standard 0.8-mm thick 4-layer FR4 substrate. The detailed operation of the developed NFC sensor hardware with a smartphone, along with its performance characteristics, including the power consumption (0.9 mW), wireless communication range (4.5 cm), and sensor characterization, has been reported by Gawade *et al.* [34].

In this work, we exploit the mechanical energy harvesting capability of the developed concertina VEH to power the front-end electronics of the NFC sensor hardware. The functional block diagram of the NFC sensor hardware assisted with the developed VEH is given in Fig. 8(a). The NFC sensor along with the AC–DC rectification unit is shown in Fig. 8(b). By connecting the VEH energy harvester, the RF energy harvested from the smartphone can be focused to facilitate the communication of the data acquired by the sensor back to the smartphone. The VEH would act as a sustainable power source, that offers the capability of continuously providing power to the electronics interface to support the NFC sensor hardware, as a replacement of batteries that only offer a limited lifetime. To pair the NFC sensor with the developed VEH, further optimizations have been performed on the hardware and the firmware of the previously reported NFC sensor. To allow for an extraction of sufficient electrical energy even from a low amplitude vibration, a double-stage voltage multiplier circuit [66], [67] comprising of two capacitors (10 μF each) and two diodes (Small-signal Schottky Diode, part number BAT85-T/R) has been employed for the rectification of the incoming AC signal from the VEH. Following the rectification stage, a 560 μF (20 V) conductive polymer aluminium solid capacitor (SEPF series) has been added to store the energy and to supply it to the NFC sensor hardware circuitry when required. The voltage regulator is activated upon receiving a minimum voltage of 2.66 V from the VEH. This regulator then provides a steady 1.8 V DC supply to the rest of the associated sensor electronics. To maintain the overall footprint of the system small, the voltage multiplier circuit along with the storage capacitor has been implemented on a PCB board mounted on

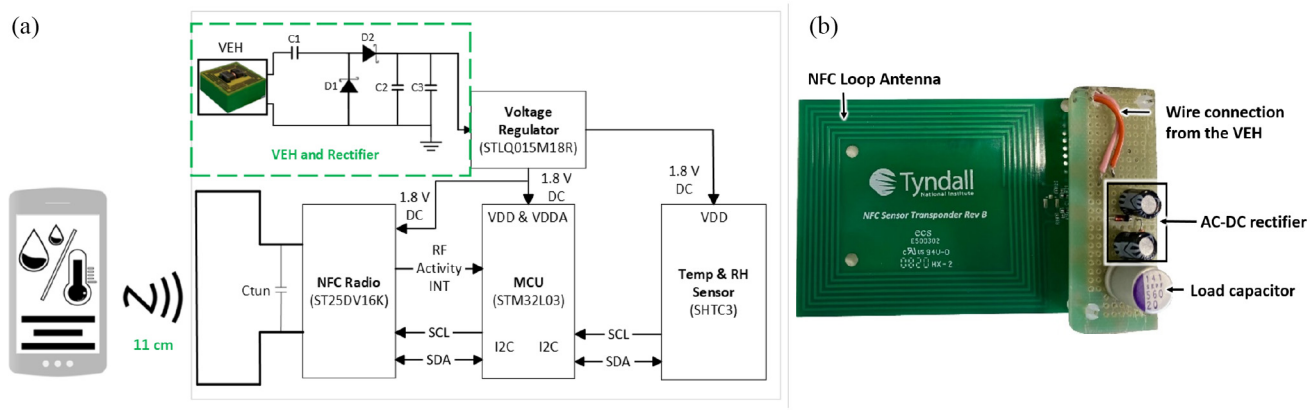

Fig. 8. (a) Functional block diagram of the NFC sensor hardware when assisted with the developed concertina VEH. (b) Developed NFC sensor hardware along with the AC–DC rectification stage integrated to facilitate the rectification of incoming AC voltage from the VEH.

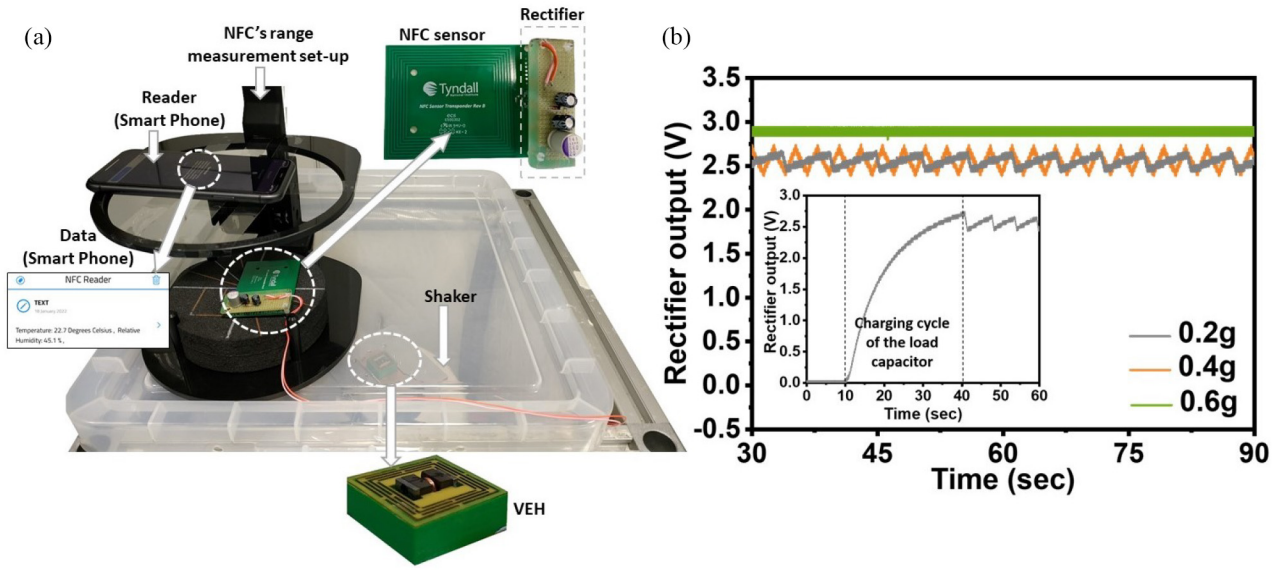

Fig. 9. (a) Experimental setup of employing the developed VEH to support the NFC sensor hardware. The VEH is placed on the shaker under the cover. (b) Variation of the rectified voltage across the load capacitor for different amplitudes of excitation of the VEH. The inset shows the fast charging cycle of the load capacitor used in this experiment.

top of the remaining electronics of the NFC sensor node with a vertical spacer. Upon the VEH integration (Fig. 8), the tapping time of the NFC sensor node has decreased from 6.79 to 1.95 s. This shorter tapping time might be attributed to the VEH supplying an adequate power to the electronics to perform continuous data acquisition and processing. Hence, the tapping time only accounts for the time taken for communicating the processed data to the reader.

V. Feasibility Experiment of Battery-Less and VEH Assisted NFC Sensor Node Platform

In this section, we demonstrate the significance of the developed concertina VEH that is implemented to assist the developed NFC sensor node platform representing an autonomous wireless platform system. The experimental setup used in this study is depicted in Fig. 9(a). The VEH is mounted on the shaker unit which emulates ambient mechanical vibrations in a laboratory environment. The shaker unit is covered with a plastic casing and on top of it a communication range measurements setup for the developed NFC hardware has been placed, which comprises a base that holds the NFC sensor hardware, and a movable stage that carries the reader (smartphone). "NFC for iPhone" and "Simply NFC" application interfaces have been used to read the data from the NFC sensor. This setup is used to vary the distance between the NFC loop antennas in the sensor hardware and that of the smartphone. The AC–DC rectifier stage, as mentioned in the previous section, has been fabricated on copper strip-board and mounted on top of the NFC hardware to minimize the length of the wired connections and to reduce the footprint. The output of the VEH is connected to the input of the rectifier stage through wired connections.

Upon applying a harmonic excitation on the VEH at the resonant frequency (75 Hz), the extracted electrical energy passes through the rectification stage and is stored into the load capacitor. Fig. 9(b) shows the variation of the rectified signal when the NFC sensor interface is connected to it as a

load. We have selected this capacitor for its fast charging capability. The amplitudes of the excitation are varied from 0.2 to 0.6 g that typically represents the amplitudes of vibrations that can be experienced on, for instance, clothes drying machine, blending machine, car dashboard [68], [69], etc. As shown in the inset of Fig. 9(b), the capacitor takes approximately 30 s to charge from 0 to 2.66 V, when such a low vibration amplitude of 0.2 g is employed. Once the voltage input to the NFC sensor hardware exceeds 2.66 V, the integrated low dropout voltage regulator (LDO) enters into the active state and provides a steady DC supply of 1.8 V to the following circuitry comprising of the microcontroller, temperature-humidity sensor along with the NFC radio transceiver. If the NFC reader (in this case a smartphone) is in the vicinity of the NFC sensor hardware, the data packet from the sensor is transmitted through the NFC radio to the reader. The energy drawn to facilitate this communication brings the voltage across the capacitor down from 2.66 to 2.4 V which puts the microcontroller and the sensors back into off mode until the capacitor charges back to 2.66 V. In the case of 0.2 g vibration, this occurs over a 4.7-s time interval. This charging and discharging of the capacitor reflects onto the rectified voltage as ripples, as shown in Fig. 9(b).

As described in Section IV, for the conventional passive NFC tags, the energy received from the reader/smartphone by the tag loop antenna, which is translated into a regulated 1.8 V DC, is partly employed to power the electronics in the NFC sensor hardware and partly for communicating (EPROM) the data-modulated signal back to the reader. The fraction of the power left for the latter then determines the strength of the load-modulated signal or equivalently the communication range of the NFC tags. For the NFC sensor hardware used in this work, it provides a communication range of 5 cm when not connected to any additional source of energy. In the case of VEH-assisted NFC tag, the VEH supplies the power required by the electronics. Therefore, the NFC sensor hardware can retain the RF power harvested from the reader fully for communicating back the sensing data-modulated signal to the reader and hence provides a larger communication range, i.e., 11 cm or 120% improvement as shown in Fig. 10(a).

Fig. 10(b) shows the variation of the deliverable power of the VEH as a function of the amplitude of excitation. The power required by the NFC sensor hardware to be fully functional is measured to be 597 μW (shown by the blue dots). It is noticed that with 0.2 g drive amplitude, 164 μW power can be extracted across the load resistance of 1 kΩ. Such a low vibration is investigated to be sufficient to support the NFC sensor leading to an increased communication range, though with a longer capacitor charging time from 2.4 V to the required 2.66 V [see Fig. 9(b)]. The obtainable energy from the VEH increases with the increasing amplitude of the external excitation. Since a larger power of 598 μW is delivered when the VEH is excited with 0.4 g acceleration (matching the required power level of the NFC sensor hardware), the capacitor charges faster between 2.4 to 2.66 V, shortening the charging time to 1.2 s as shown in Fig. 9(b), while extending the communication range up to 11 cm. It is interesting to note that by further increasing the amplitude of excitation, e.g., for 0.6 g, the VEH provides substantial energy which drives

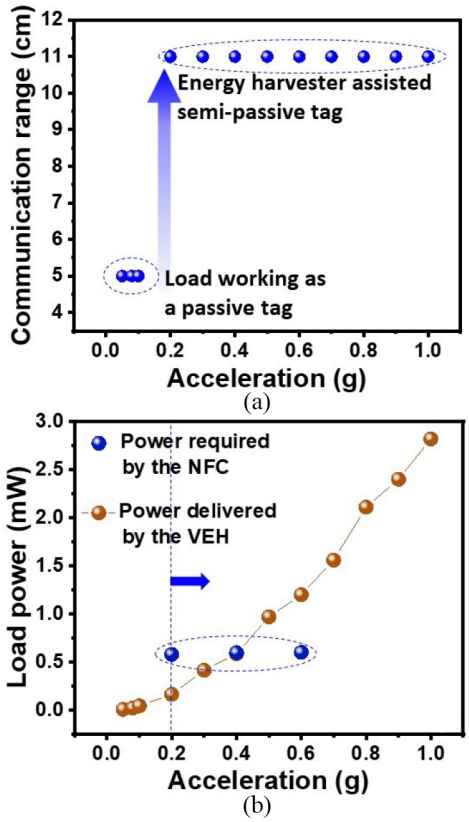

Fig. 10. (a) Demonstrates the variation of the communication range of the NFC hardware as a function of the amplitude of excitation. (b) Shows the variation of the power delivered by the VEH across the optimized load as a function of the acceleration. The blue points show the power consumption of the NFC sensor hardware when the amplitude of excitation for the VEH changes from 0.2 g to 0.6 g.

the NFC sensor hardware interface autonomously, thereby implementing a sustainable power source to support the NFC hardware. In Fig. 9(b) the steady supply from the rectification stage (green line) indicates that the capacitor at this stage would no longer be required to store and supply energy to the circuitry associated with the NFC.

VI. Comparison With the State-of-the-Art VEHs and Envisaged IoT Application

A comparison of the performance of the developed VEH with the state-of-the-art VEHs has been presented in Table III. The key parameters of comparison are the footprint of the VEH device used to power the wireless platform, the amplitude of excitation, the power density (delivered power per unit volume per unit excitation), and the charge storage capacitor. The table shows that, in terms of the footprint, the developed VEH device outpaces all the rest of the devices. Additionally, the device starts to power the wireless sensor node at a very low level of acceleration which makes this suitable for a wide range of IoT-based application scenarios. The wireless communication system has also been developed and optimized carefully to minimize the power consumption so that the autonomous wireless platform with enhanced communication range is functional even for weak vibrations. To the author's

TABLE III
PERFORMANCE COMPARISON OF THE DEVELOPED PROTOTYPE WITH THE REPORTED VEHS

Ref.	Excitation (g)	Resonant frequency(Hz)	Volume (cm^3)	Delivered power (μW)	Power density ($\mu W/cm^3g^2$)	Communication protocol	Load capacitance(μF)
EM (resonant) [32]	$\sim$ 0.5	33	123.75	$\sim$ 800	25.8	Radio Transceiver Short-burst 2.4GHz proprietary	23.5
EM (resonant) [31]	3	6	420	119000	31.5	No demonstration with wireless sensor platform	680
PE (resonant) [29]	0.25	100	200	$\sim$ 4000	320	Radio Transceiver	500
PE (resonant) [26]	0.2	39,110	NA	$\sim$ 3800	NA	Radio Transceiver	100
EM (resonant) [24]	$\sim$ 0.5	28,40	$\sim$ 206	6500	126.2	No demonstration with wireless sensor platform	NA
EM+TE (resonant) [12]	0.6	4.5	$\sim$ 29.3	10070	954.7	Directly powered portable electronics	22
EM (resonant) [11]	0.73	13	$\sim$ 93	980	19.77	LoRaWAN and BLE	Supercapacitor
This work	0.2	75	9	164	455.6	NFC	560
This work	0.6	75	9	1200	370.36	NFC	Not required

Note: EM- Electromagnetic, PE- Piezoelectric, TE-Triboelectric, NA- Not Available

best knowledge, this work is a first of its nature presenting a detailed feasibility study of combining high-efficiency VEH with emerging the NFC technology to implement a robust and sustainable wireless communication platform for IoT applications.

As demonstrated, the developed concertina-VEH is sensitive to low levels of vibrations which enables this energy harvesting system to transduce mechanical energy even from the weak vibrations, opening up the scope for exploiting this benefit in some niche application areas. For example, in the context of industrial cleanroom environments, continuous monitoring of temperature and relative humidity, and maintaining their variation range between 18 °C–21 °C and 30%–50%, respectively, is an imperative requirement for minimizing microbial growth, static charge build up, delicate equipment damage as well as for the users comfort [70]. The heating, ventilation, and air conditioning (HVAC) units installed inside the cleanroom offers substantial mechanical energy distributed around the resonant frequency of the concertina-VEH [19], [71]. In the context of the above-mentioned application scenario, the mechanical energy from the HVAC system will be consistently available since the HVAC in a clean room has to be operational all the time to keep the contaminants at a minimum, which ensures perpetual mechanical energy extraction through the concertina-VEH. This opens up the scope for installing the developed concertina-VEH on the HVAC systems which would enable the harvester to generate substantial energy. The delivered power through the harvester could be employed to power the electronics interface of the NFC-based sensor node, while enhancing the range of communication of the NFC node. Hence, the developed NFC sensor node could report on the vital physical parameters of the cleanroom environment while being assisted through the concertina-VEH which would harness mechanical energy from the ceiling HVAC units.

The presented concertina spring topology offers the unique scope of tuning the natural frequency of oscillation of the device by adding more stages of concertina springs. Such flexibility could be well exploited for niche application areas, such as harnessing mechanical energy from the human body by scaling down the frequency, typically less than 10 Hz, through additional stages of concertina springs. NFC sensor system could be implemented on flexible material [72], [73] for the ease of integration on the human body. The concertina VEHs together with flexible NFC sensor system could implement a sustainable and robust wireless platform for human health monitoring. The successful demonstration of the developed concertina VEH supporting the constructed NFC sensor node also implies a possible avenue to implement the VEH for other types of wireless communication platform. This includes those-based on the far-field communication (e.g., [74] and [75]) to allow for the development of a sustainable and robust wireless sensing systems with an even higher communication range.

VII. CONCLUSION

A battery-less VEH-assisted NFC sensor node has been reported. The resonant FR4-based VEH comprises interleaved springs that are connected in series, building a concertina shape that exhibits a large amplitude of displacement (2.5 mm) within a small footprint of 9 cm^3 when subjected to external excitation. Owing to this enhanced out-of-plane compliance, the VEH offers a large power density of 455.6 $\mu W/cm^3g^2$ when operating at the resonance. This

makes the concertina-VEH a potential candidate for assisting the developed low-power consuming NFC sensor node. With the VEH powering the electronic interface of the sensor node, the electromagnetic interaction between the transmitting antenna and the reader embedded in the smartphone enhances which in turn brings a 120% improvement in the range of communication of this wireless sensor node. The excellent dynamic response of the concertina-VEH enables it to effectively harness mechanical energy even from weaker vibrations (e.g., 0.2 g harmonic excitation). For lower amplitudes of excitation, a storage capacitor of 560 μF has been used to provide a steady DC supply to the sensor interface. But for moderate acceleration levels (0.6 g), the concertina-VEH generates considerably large power (1.2 mW), making the capacitor redundant for steadily powering the sensor electronics.

REFERENCES

[1] A. Zanella, N. Bui, A. Castellani, L. Vangelista, and M. Zorzi, "Internet of Things for smart cities," *IEEE Internet Things J.*, vol. 1, no. 1, pp. 22–32, Feb. 2014.

[2] K. Ashton, "That 'Internet of Things' thing," *RFID J.*, vol. 22, no. 7, pp. 97–114, 2009.

[3] A. Adeel *et al.*, "A survey on the role of wireless sensor networks and IoT in disaster management," in *Geological Disaster Monitoring Based on Sensor Networks*. Singapore: Springer, 2019.

[4] F. Akhter, H. R. Siddiquei, M. E. E. Alahi, and S. C. Mukhopadhyay, "Design and development of an IoT-enabled portable phosphate detection system in water for smart agriculture," *Sens. Actuators A, Phys.*, vol. 330, Oct. 2021, Art. no. 112861.

[5] L. Zhao, I. B. M. Matsuo, Y. Zhou, and W. Lee, "Design of an industrial IoT-based monitoring system for power substations," *IEEE Trans. Ind. Appl.*, vol. 55, no. 6, pp. 5666–5674, Nov./Dec. 2019.

[6] H. Huang, X. Li, S. Liu, S. Hu, and Y. Sun, "TriboMotion: A self-powered triboelectric motion sensor in wearable Internet of Things for human activity recognition and energy harvesting," *IEEE Internet Things J.*, vol. 5, no. 6, pp. 4441–4453, Dec. 2018.

[7] P. Li, Z. Long, and Z. Yang, "RF energy harvesting for battery-less and maintenance-free condition monitoring of railway tracks," *IEEE Internet Things J.*, vol. 8, no. 5, pp. 3512–3523, Mar. 2021.

[8] "Perpetuum Rail Applications." Jul. 7, 2022. [Online]. Available: https://perpetuum.com/applications/rail/

[9] M. Koca, G. Gurbilek, B. Soner, and S. Coleri, "Empirical feasibility analysis for energy harvesting intravehicular wireless sensor networks," *IEEE Internet Things J.*, vol. 8, no. 1, pp. 179–186, Jan. 2021.

[10] K. Paul, A. Amann, and S. Roy, "Tapered nonlinear vibration energy harvester for powering Internet of Things," *Appl. Energy*, vol. 283, Feb. 2021, Art. no. 116267.

[11] J. C. Rodriguez, V. Nico, and J. Punch, "A vibration energy harvester and power management solution for battery-free operation of wireless sensor nodes," *Sensors*, vol. 19, no. 17, p. 3776, 2019.

[12] M. Salauddin, R. M. Toyabur, P. Maharjan, and J. Y. Park, "High performance human-induced vibration driven hybrid energy harvester for powering portable electronics," *Nano Energy*, vol. 45, pp. 236–246, Mar. 2018.

[13] D. Mallick, P. Constantinou, P. Podder, and S. Roy, "Multi-frequency MEMS electromagnetic energy harvesting," *Sens. Actuators A, Phys.*, vol. 264, pp. 247–259, Sep. 2017.

[14] L. Zuo, B. Scully, J. Shestani, and Y. Zhou, "Design and characterization of an electromagnetic energy harvester for vehicle suspensions," *Smart Mater. Struct.*, vol. 19, no. 4, 2010, Art. no. 45003.

[15] D. Mallick, A. Amann, and S. Roy, "A nonlinear stretching based electromagnetic energy harvester on FR4 for wideband operation," *Smart Mater. Struct.*, vol. 24, no. 1, 2014, Art. no. 15013.

[16] Y. Zhao, X. Ling, Z. Wang, W. Gong, and G. Li, "Acceleration frequency characteristics of the freight-train-induced vibration of the Beijing-Harbin railway subgrade," *Shock Vib.*, vol. 2020, Nov. 2020, Art. no. 6651713.

[17] C. Pronello, "Analysis of tram-induced vibrations affecting roads and buildings in standard urban sites," *Int. J. Acoust. Vib.*, vol. 8, no. 1, pp. 21–29, 2003.

[18] J. T. Gaunt and C. D. Sutton, "Highway bridge vibration studies," Dept. Civil Eng., Purdue Univ., West Lafayette, IN, USA, Rep. JHRP-75-2, 1981.

[19] G. Iannace, G. Ciaburro, and A. Trematerra, "Heating, ventilation, and air conditioning (HVAC) noise detection in open-plan offices using recursive partitioning," *Buildings*, vol. 8, no. 12, p. 169, 2018.

[20] P. L. Green, E. Papatheou, and N. D. Sims, "Energy harvesting from human motion and bridge vibrations: An evaluation of current nonlinear energy harvesting solutions," *J. Intell. Mater. Syst. Struct.*, vol. 24, no. 12, pp. 1494–1505, 2013.

[21] D. Zhu and S. Beeby, "A broadband electromagnetic energy harvester with a coupled bistable structure," *J. Phys. Conf. Series*, vol. 476, no. 1, 2013, Art. no. 12070.

[22] F. M. Foong, C. K. Thein, and D. Yurchenko, "Important considerations in optimising the structural aspect of a SDOF electromagnetic vibration energy harvester," *J. Sound Vib.*, vol. 482, Sep. 2020, Art. no. 115470.

[23] L. Dhakar, H. Liu, F. E. H. Tay, and C. Lee, "A new energy harvester design for high power output at low frequencies," *Sens. Actuators A, Phys.*, vol. 199, pp. 344–352, Sep. 2013.

[24] M. Perez, S. Chesné, C. Jean-Mistral, K. Billon, R. Augez, and C. Clerc, "A two degree-of-freedom linear vibration energy harvester for tram applications," *Mech. Syst. Signal Process.*, vol. 140, Jun. 2020, Art. no. 106657.

[25] R. Torah, P. Glynne-Jones, M. Tudor, T. O'Donnell, S. Roy, and S. Beeby, "Self-powered autonomous wireless sensor node using vibration energy harvesting," *Meas. Sci. Technol.*, vol. 19, no. 12, 2008, Art. no. 125202.

[26] S. Lee, B. D. Youn, and B. C. Jung, "Robust segment-type energy harvester and its application to a wireless sensor," *Smart Mater. Struct.*, vol. 18, no. 9, 2009, Art. no. 95021.

[27] "Revibe energy harvester," Data Sheet, ReVibe Energy, Göteborg, Sweden, Jul. 2022. [Online]. Available: https://revibeenergy.com/modeld/

[28] D. Mallick and S. Roy, "Bidirectional electrical tuning of FR4 based electromagnetic energy harvesters," *Sens. Actuators A, Phys.*, vol. 226, pp. 154–162, May 2015.

[29] E. K. Reilly, F. Burghardt, R. Fain, and P. Wright, "Powering a wireless sensor node with a vibration-driven piezoelectric energy harvester," *Smart Mater. Struct.*, vol. 20, no. 12, 2011, Art. no. 125006.

[30] J. Qiu, X. Liu, H. Chen, X. Xu, Y. Wen, and P. Li, "A low-frequency resonant electromagnetic vibration energy harvester employing the halbach arrays for intelligent wireless sensor networks," *IEEE Trans. Magn.*, vol. 51, no. 11, pp. 1–4, Nov. 2015.

[31] M. Gao, P. Wang, Y. Cao, R. Chen, and D. Cai, "Design and verification of a rail-borne energy harvester for powering wireless sensor networks in the railway industry," *IEEE Trans. Intell. Transp. Syst.*, vol. 18, no. 6, pp. 1596–1609, Jun. 2017.

[32] O. Rubes, J. Chalupa, F. Ksica, and Z. Hadas, "Development and experimental validation of self-powered wireless vibration sensor node using vibration energy harvester," *Mech. Syst. Signal Process.*, vol. 160, Nov. 2021, Art. no. 107890.

[33] D. R. Gawade *et al.*, "A museum artefact monitoring testbed using LoRaWAN," in *Proc. IEEE Symp. Comput. Commun. (ISCC)*, 2021, pp. 1–3.

[34] D. R. Gawade *et al.*, "A smart archive box for museum artifact monitoring using battery-less temperature and humidity sensing," *Sensors*, vol. 21, no. 14, p. 4903, 2021.

[35] C. Peres, M. Emam, H. Jafarzadeh, M. Belcastro, and B. O'Flynn, "Development of a low-power underwater NFC-enabled sensor device for seaweed monitoring," *Sensors*, vol. 21, no. 14, p. 4649, 2021.

[36] P. Escobedo, M. Bhattacharjee, F. Nikbakhtnasrabadi, and R. Dahiya, "Smart bandage with wireless strain and temperature sensors and batteryless NFC tag," *IEEE Internet Things J.*, vol. 8, no. 6, pp. 5093–5100, Mar. 2021.

[37] X. Qian, Z. Li, Z. Meng, N. Gao, and Z. Zhang, "Flexible RFID Tag for sensing the total minerals in drinking water via smartphone tapping," *IEEE Sensors J.*, vol. 21, no. 21, pp. 24749–24758, Nov. 2021.

[38] "Application Note: NFC / RFID, ST25 Product Overview." Jul. 7, 2022. [Online]. Available: https://www.st.com/content/ccc/resource/sales_and_marketing/presentation/product_presentation/group1/a9/5d/77/96/be/9a/48/7e/ST25_NFC_RFID_product_overview/files/ST25_product_overview.pdf/jcr:content/translations/en.ST25_product_overview.pdf

[39] D. R. Gawade *et al.*, "A battery-less NFC sensor transponder for museum artefact monitoring-a review of NFC sensor technology and a proposed solution," in *Proc. Sensorcomm*, 2019, pp. 89–96.

[40] P. Escobedo *et al.*, "Smart facemask for wireless CO2 monitoring," *Nat. Commun.*, vol. 13, no. 1, pp. 1–12, 2022.
[41] R. Raju, G. E. Bridges, and S. Bhadra, "Wireless passive sensors for food quality monitoring: Improving the safety of food products," *IEEE Antennas Propag. Mag.*, vol. 62, no. 5, pp. 76–89, Oct. 2020.
[42] P. Escobedo *et al.*, "Flexible passive near field communication tag for multigas sensing," *Anal. Chem.*, vol. 89, no. 3, pp. 1697–1703, 2017.
[43] C. Strangfeld, S. Johann, and M. Bartholmai, "Smart RFID sensors embedded in building structures for early damage detection and long-term monitoring," *Sensors*, vol. 19, no. 24, p. 5514, 2019.
[44] X. Hu, L. Xu, X. Lin, and M. Pecht, "Battery lifetime prognostics," *Joule*, vol. 4, no. 2, pp. 310–346, 2020.
[45] D. Grech, K. S. Kiang, J. Zekonyte, M. Stolz, R. J. K. Wood, and H. M. H. Chong, "Highly linear and large spring deflection characteristics of a quasi-concertina MEMS device," *Microelectron. Eng.*, vol. 119, pp. 75–78, May 2014.
[46] D. Grech *et al.*, "A quasi-concertina force-displacement MEMS probe for measuring biomechanical properties," *Sens. Actuators A, Phys.*, vol. 275, pp. 67–74, Jun. 2018.
[47] Y. Li, J. Li, A. Yang, Y. Zhang, B. Jiang, and D. Qiao, "Electromagnetic vibrational energy harvester with microfabricated springs and flexible coils," *IEEE Trans. Ind. Electron.*, vol. 68, no. 3, pp. 2684–2693, Mar. 2021.
[48] D. Mallick, A. Amann, and S. Roy, "High figure of merit nonlinear microelectromagnetic energy harvesters for wideband applications," *J. Microelectromech. Syst.*, vol. 26, no. 1, pp. 273–282, 2016.
[49] S. Sun, X. Dai, Y. Sun, X. Xiang, G. Ding, and X. Zhao, "MEMS-based wide-bandwidth electromagnetic energy harvester with electroplated nickel structure," *J. Micromech. Microeng.*, vol. 27, no. 11, 2017, Art. no. 115007.
[50] F. Khan, F. Sassani, and B. Stoeber, "Copper foil-type vibration-based electromagnetic energy harvester," *J. Micromech. Microeng.*, vol. 20, no. 12, 2010, Art. no. 125006.
[51] P. Wang, K. Tanaka, S. Sugiyama, X. Dai, X. Zhao, and J. Liu, "A micro electromagnetic low level vibration energy harvester based on MEMS technology," *Microsyst. Technol.*, vol. 15, no. 6, pp. 941–951, 2009.
[52] Z. Yang, N. Ismail, C. Son, P. M. Ferreira, and S. Kim, "Broadband, tunable, miniaturized vibration energy harvester using nonlinear elastomer beams and stretchable interconnects," *Adv. Mater. Technol.*, vol. 4, no. 12, 2019, Art. no. 1900783.
[53] P. Podder, A. Amann, and S. Roy, "A bistable electromagnetic micropower generator using FR4-based folded arm cantilever," *Sens. Actuators A, Phys.*, vol. 227, pp. 39–47, May 2015.
[54] G. Hatipoglu and H. Ürey, "FR4-based electromagnetic energy harvester for wireless sensor nodes," *Smart Mater. Struct.*, vol. 19, no. 1, 2009, Art. no. 15022.
[55] G. Aldawood, H. T. Nguyen, and H. Bardaweel, "High power density spring-assisted nonlinear electromagnetic vibration energy harvester for low base-accelerations," *Appl. Energy*, vol. 253, Nov. 2019, Art. no. 113546.
[56] S. P. Beeby *et al.*, "A micro electromagnetic generator for vibration energy harvesting," *J. Micromech. Microeng.*, vol. 17, no. 7, pp. 1257–1265, 2007.
[57] P. White and M. Roland, "Near field communication (NFC) technology and measurements," White Paper, Rohde Schwarz, Münich, Germany, 2011. [Online]. Available: https://cdn.rohde-schwarz.com.cn/pws/dl_downloads/dl_application/application_notes/1ma182/1MA182_5E_NFC_WHITE_PAPER.pdf
[58] S. Popli, R. K. Jha, and S. Jain, "A survey on energy efficient narrowband Internet of Things (NBIoT): Architecture, application and challenges," *IEEE Access*, vol. 7, pp. 16739–16776, 2018.
[59] "Quectel BC95-G multi-band NB-IoT module with ultra-low power consumption," Data Sheet, Quectel, Shanghai, China, Jul. 2022. [Online].Available: https://www.quectel.com/wp-content/uploads/pdfupload/Quectel_BC95-G_NB-IoT_Specification_V1.9.pdf
[60] "S2-LP ultra-low power, high performance, sub1 GHz transceiver," Data Sheet, STMicroelectronics, Geneva, Switzerland, Jul. 7, 2022. [Online]. Available: https://www.st.com/en/wireless-connectivity/s2-lp.html
[61] "CMWX1ZZABZ-078," Data Sheet, Murata Manuf., Kyoto, Japan, Jul. 7, 2022. [Online].Available: https://content.arduino.cc/assets/mkrwan1310-murata_lora_module-type_abz.pdf
[62] "CC3200 simplelink Wi-Fi and Internet-of-Things solution, a single-chip wireless MCU," Data Sheet, Texas Instrum., Dallas, TX, USA, Jul. 2022. [Online]. Available: https://www.ti.com/lit/ds/symlink/cc3200.pdf
[63] "Application Note: Zolertia RE-Mote." Jul. 7, 2022. [Online]. Available: https://github-wiki-see.page/m/Zolertia/Resources/wiki/RE-Mote
[64] Z. Jianyong, L. Haiyong, C. Zili, and L. Zhaohui, "RSSI based Bluetooth low energy indoor positioning," in *Proc. Int. Conf. Indoor Position. Indoor Navigation (IPIN)*, 2014, pp. 526–533.
[65] "nRF52840, Product Specification." Nordic Semiconductor. Jul. 7, 2022. [Online]. Available: https://infocenter.nordicsemi.com/pdf/nRF52840_PS v1.2.pdf
[66] S. Filiz and U. Yunus, "A comparative study: Voltage multipliers for RF energy harvesting system," *Commun. Faculty Sci. Univ. Ankara Series A2-A3 Phys. Sci. Eng.*, vol. 61, no. 1, pp. 12–23, 2019.
[67] S. S. Chouhan, M. Nurmi, and K. Halonen, "Efficiency enhanced voltage multiplier circuit for RF energy harvesting," *Microelectron. J.*, vol. 48, pp. 95–102, Feb. 2016.
[68] S. Roundy, P. K. Wright, and J. Rabaey, "A study of low level vibrations as a power source for wireless sensor nodes," *Comput. Commun.*, vol. 26, pp. 1131–1144, Jul. 2003.
[69] D. Bhatia *et al.* "Continuous scavenging of broadband vibrations via omnipotent tandem triboelectric nanogenerators with cascade impact structure," *Sci. Rep.*, vol. 9, pp. 1–9, Jun. 2019.
[70] T. Sandle. "A Humidex For The Cleanroom: Why Temperature And Humidity Control Matters." Jul. 7, 2022. [Online]. Available: https://www.ivtnetwork.com/article/humidex-cleanroom-why-temperature-and-humidity-control-matters
[71] Y. Hu and Y. Xu, "A wideband vibration energy harvester based on a folded asymmetric gapped cantilever," *Appl. Phys. Lett.*, vol. 104, no. 5, 2014, Art. no. 53902.
[72] A. Noda, "Wearable NFC reader and sensor tag for health monitoring," in *Proc. IEEE Biomed. Circuits Syst. Conf. (BioCAS)*, 2019, pp. 1–4.
[73] M. Zulqarnain *et al.*, "A flexible ECG patch compatible with NFC RF communication," *NPJ Flexible Electron.*, vol. 4, no. 1, p. 13, 2020.
[74] S. N. R. Kantareddy, I. Mathews, R. Bhattacharyya, I. M. Peters, T. Buonassisi and S. E. Sarma, "Long range battery-less PV-powered RFID tag sensors," *IEEE Internet Things J.*, vol. 6, no. 4, pp. 6989–6996, Aug. 2019.
[75] A. Sharif *et al.*, "Low-cost inkjet-printed UHF RFID tag-based system for Internet of Things applications using characteristic modes," *IEEE Internet Things J.*, vol. 6, no. 2, pp. 3962–3975, Apr. 2019.

Kankana Paul received the B.Sc. (Hons.) degree in physics and the B.Tech. and M.Tech. degrees in radiophysics and electronics engineering from the University of Calcutta, Kolkata, India, in 2012, 2015, and 2017, respectively.

She joined Tyndall National Institute, University College Cork, Cork, Ireland, in 2017 November, as a Doctoral Research Student and she is currently holding that position. Her research interest includes development of electromagnetic vibrational energy harvester, next-generation magnetic material for CMOS compatible integration with MEMS scale vibration energy harvester, optimization of magnetic performance through analytical, and numerical modeling.

Dinesh R. Gawade (Member, IEEE) received the Bachelor of Technology degree in electronics and communication technology from the Department of Technology, Shivaji University, India, in 2016. He is currently pursuing the M.Eng.Sc. degree with the Antenna and RF Design Team, WSN Group, Tyndall National Institute, Cork, Ireland.

After graduation, he worked in the electronics industry for couple of years as a Hardware Design Engineer from 2016 to 2018. He then worked with the Indian Institute of Technology Mandi, Mandi, India, as a Project Engineer (Hardware design) before joining Tyndall National Institute, University College Cork, Cork, Ireland, in 2019. His research interest includes development of battery-less sensing devices, low power sensor node, and long range wireless sensor network.

Roy B. V. B. Simorangkir (Member, IEEE) received the Ph.D. degree in electronic engineering from Macquarie University, Sydney, NSW, Australia, in 2018.

He held a Teaching Staff position with Macquarie University International College, Macquarie Park, NSW, Australia, from March 2018 to May 2019. He was also with the Reconfigurable Electronics and Antennas Research Group, Macquarie University as a Postdoctoral Researcher from September 2018 to December 2018. From May 2019 to May 2020, he worked as a Postdoctoral Researcher with the Institute of Electronics and Telecommunications of Rennes, University of Rennes 1, Rennes, France. He is currently with the Wireless Sensor Networks Group, Tyndall National Institute, University College Cork, Cork, Ireland, as a Postdoctoral researcher. His general research interests include design and fabrication of flexible antennas and sensors, reconfigurable antennas, and ultra-wideband (UWB) antennas.

Dr. Simorangkir is currently serving as a Guest Editor of a Special Issue of Sensors Journal (MDPI) and Electronics Journal (MDPI). In 2017, one of his works won the First Place in the IEEE Region 10 Student Paper Contest, Postgraduate Category, and was selected as a Finalist in the Student Paper and Advanced Practice Paper Competitions of the IEEE MTT-S International Microwave Symposium, Honolulu. He has been serving as a regular reviewer for several reputable journals in his research field. He was a Session Chair of the 2018 ACES Symposium, Beijing, and the 2021 IEEE International Symposium on Antennas and Propagation, Singapore.

Brendan O'Flynn (Senior Member, IEEE) received the B.Eng. (Hons.), M.Eng.Sc., and Ph.D. degrees from University College Cork, Cork, Ireland, in 1993, 1995, and 2016, respectively.

He is currently a Senior Staff Researcher with Tyndall National Institute, Cork. He is also the Head of the Wireless Sensor Networks Group. His research interests include wearable sensing systems, edge-based analytics, sensor system integration, low-power embedded systems design and development, system miniaturization, and RF system design and optimization. He has published widely in these areas and has secured significant funding for the development and deployment of "Smart Sensing" technologies and applied research projects.

John L. Buckley (Member, IEEE) was born in Cork, Ireland. He received the B.Eng. degree from Cork Institute of Technology, Cork, Ireland, in 1994, the M.Eng.Sc. degree from University College Cork, Cork, in 2004, and the Ph.D. degree from the Department of Electrical and Electronic Engineering, University College Cork in 2016.

He was with EMC Corporation, Cork, from 1994 to 2002 and joined the Tyndall National Institute, University College Cork in 2005. He is a Senior Researcher and Team Leader for the Antennas and RF Team, WSN Group. His research interests include antenna design and measurement, wearable and implantable antenna design, and EM and RF circuit modeling for wireless applications.

Andreas Amann received the Diploma degree in physics from the University of Bonn, Bonn, Germany, in 1998, and the Ph.D. degree in physics from the Technical University of Berlin, Berlin, Germany, in 2003.

After being a Visiting Researcher with the Institute of Applied Optics, Florence, Italy, and a Postdoctoral Researcher with Tyndall National Institute, Cork, Ireland, He is currently a Senior Lecturer with the School of Mathematical Sciences, University College Cork, Cork, Ireland. His research interest include nonlinear dynamics, mathematical modeling, and machine learning.

Saibal Roy received the M.Sc. degree in physics from the Indian Institute of Technology (IIT) Khraragpur, Khraragpur, India, in 1987, and the Ph.D. degree in physics/materials science from Indian Association for the Cultivation of Science, Kolkata, India, in 1994.

He is a Research Professor with the Department of Physics, National University of Ireland—University College Cork, Cork, Ireland, and the Head of Micropower Devices and Nanomagnetics Research Group, Tyndall National Institute, Cork. He is a Science Foundation Ireland Principal Investigator and a Funded Investigator in a research center on "Future communication, network, and sustainable IoT—CONNECT." He is particularly known internationally in the area of integrated high-frequency magnetics for "power supply on chip," renewable MEMS energy harvesting through electromagnetic transduction (EMT) and demonstration of unconventional magnetic properties in different "nano-hetero-structures" leading to "More than Moore" functional devices. Some of his published works on "Miniaturized vibrational energy harvesting through EMT" have received >2000 citations to date and featured widely in international media. On the other hand, Tyndall "Magnetics on Si" team successfully licensed the batch-fabricated micro-transformers/micro-inductors capable of operating at 100 s of MHz for the "power supply on chip" technology to three major multinational companies with a substantial license fee. He has supervised 40 researchers to date, while many of them received different national and international awards and currently holding senior positions in academia as well as in multinational companies. He has three granted global patents, authored/coauthored seven book chapters and published 200 papers in leading journals and conference proceedings, with over 6500 citations and H-index of 38 to date.

Prof. Roy was awarded the coveted A. S. Paintal Chair Professor of Engineering, the Prof. Tom Brazil Excellence in Research Award, and the GIAN Fellow. In recognition, the team was awarded as the Research Team of the year by the University.